Published in final edited form as:
Biochemistry. 2012 April 10; 51(14): 3011–3020. doi:10.1021/bi201827a.

Structure of 2-methylisoborneol synthase from *Streptomyces coelicolor* and implications for the cyclization of a non-canonical *C*-methylated monoterpenoid substrate†

Mustafa Köksal[§], **Wayne K. W. Chou**[#], **David E. Cane**[#], and **David W. Christianson**[§,*]

[§]Roy and Diana Vagelos Laboratories, Department of Chemistry, University of Pennsylvania, 231 South 34th Street, Philadelphia, PA 19104-6323 USA

[#]Department of Chemistry, Brown University, Box H, Providence, RI 02912-9108 USA

Abstract

The crystal structure of 2-methylisoborneol synthase (MIBS) from *Streptomyces coelicolor* A3(2) has been determined in complex with substrate analogues geranyl-*S*-thiolodiphosphate and 2-fluorogeranyl diphosphate at 1.80 Å and 1.95 Å resolution, respectively. This terpenoid cyclase catalyzes the cyclization of the naturally-occuring, non-canonical *C*-methylated isoprenoid substrate, 2-methylgeranyl diphosphate, to form the bicyclic product 2-methylisoborneol, a volatile C_{11} homoterpene alcohol with an earthy, musty odor. While MIBS adopts the tertiary structure of a class I terpenoid cyclase, its dimeric quaternary structure differs from that previously observed in dimeric terpenoid cyclases from plants and fungi. The quaternary structure of MIBS is nonetheless similar in some respects to that of dimeric farnesyl diphosphate synthase, which is not a cyclase. The structures of MIBS complexed with substrate analogues provide insights regarding differences in the catalytic mechanism of MIBS and the mechanisms of (+)-bornyl diphosphate synthase and *endo*-fenchol synthase, plant cyclases that convert geranyl diphosphate into products with closely related bicyclic bornyl skeletons, but distinct structures and stereochemistries.

With more than 60,000 compounds identified to date, terpenoids (also known as terpenes or isoprenoids) comprise the largest and most diverse family of natural products (Dictionary of Natural Products: http://dnp.chemnetbase.com). The structural and stereochemical complexity of terpenoid natural products largely results from the catalytic activity of terpenoid cyclases (1-8). These fascinating enzymes generate a highly reactive carbocation in an acyclic isoprenoid substrate, either by triggering the ionization of an isoprenoid allylic diphosphate group or by protonating an isoprenoid C=C bond (or derived epoxide), to initiate a multi-step, electrophilic cyclization cascade ultimately terminated by proton abstraction or through capture of water by the final carbocation intermediate.

In general, terpenoids contain one or more 5-carbon isoprenoid units and are named accordingly. For example, hemiterpenes contain a single isoprenoid unit (C_5), monoterpenes contain two isoprenoid units (C_{10}), sesquiterpenes contain three isoprenoid units (C_{15}), and so on. Even so, in the course of a typical biosynthetic pathway additional modifications occur, such as oxidation, *O*-methylation, and esterification, that may alter the total number of carbon atoms in the final terpenoid natural product. Such modifications almost always

†Supported by US National Institutes of Health Grants GM56838 (D.W.C.) and GM30301 (D.E.C)

*To whom correspondence should be addressed. D.W.C.: telephone: (215) 898-5714; fax: (215) 573-2201; chris@sas.upenn.edu.

Supporting Information Available Product profiles for wild-type, E193A, and Y69F MIBS. This material is available free of charge via the Internet at http://pubs.acs.org.

result from biosynthetic steps that follow the initial terpenoid cyclization reaction, since terpenoid cyclases usually utilize a very small number of common acyclic substrates containing an integral number of 5-carbon isoprenoid units. The carbon content of a canonical substrate is C_{5n} with n = 1, 2, 3…, for example, as found in geranyl diphosphate (C_{10}) or farnesyl diphosphate (C_{15}). In recent explorations of substrate promiscuity and biosynthetic diversity, however, it has been observed that terpenoid cyclases can occasionally process synthetically modified isoprenoid substrates. For example, aristolochene synthase not only catalyzes the cyclization of 6,7-dihydrofarnesyl diphosphate to form dihydrogermacrene A (9), but it can also convert various fluorinated farnesyl diphosphate analogues into the corresponding fluorinated analogues of germacrene A (10, 11). In another example, incubation of trichodiene synthase with 4-methylfarnesyl diphosphate yields multiple methylated sesquiterpene (C_{16}) products (12). Therefore, it is possible for a modified isoprenoid substrate to be accommodated and catalytically processed in a terpenoid cyclase active site.

Significantly, terpene synthases that catalyze the cyclization of a naturally-occurring, non-canonical (i.e., C_m, $m \neq 5n$, n = 1, 2, 3…) isoprenoid substrate have recently been discovered. A wide variety of soil bacteria, including *Streptomyces coelicolor* A3(2), *S. lasaliensis*, *S. griseus*, *S. ambofaciens*, and *Saccharopolyspora erythraea* generate 2-methylisoborneol (Figure 1), a volatile C_{11} terpene alcohol that, along with the degraded sesquiterpene geosmin, is responsible for the characteristic odor of moist soil (13). Although 2-methylisoborneol produced by various cyanobacteria is a major contributor to malodorous off-flavor in infected fish and other products of aquaculture, as well as unpleasant musty tastes in contaminated drinking water (14-16), it is also the source of the pleasing earthy aromas of Brie and Camembert cheeses (17). 2-Methylisoborneol is generated by the cyclization of the methylated isoprenoid substrate, 2-methylgeranyl diphosphate (2MGPP)[1], in a reaction catalyzed by 2-methylisoborneol synthase (MIBS) (18, 19).[2] Importantly, MIBS was the first terpenoid cyclase to be discovered that utilizes a non-canonical but naturally-occurring isoprenoid substrate. The identification of MIBS in other bacteria and cyanobacteria, as well as the closely related 2-methylenebornane synthase from *Pseudomonas fluorescens* PfO-1 and *Micromonospora olivasterospora* (19-22), clearly indicates a wider, previously unsuspected role for terpenoid cyclases that can function with non-canonical isoprenoid substrates. Indeed, more than 25 confirmed or likely orthologues of MIBS and 2-methylenebornane synthase are evident in the unified protein databases.

The amino acid sequence of MIBS from *S. coelicolor* reveals the presence of **D**^{197}DCYCE**D** and **N**^{345}DLY**S**YTK**E** motifs, which correspond to the universally conserved metal-binding motifs characteristic of nearly all class I terpenoid cyclases (boldface indicates putative metal-binding residues) (3, 4). These motifs typically bind the three Mg^{2+} ions that are required for catalysis. As a class I terpenoid cyclase, MIBS is therefore expected to initiate the formation of 2-methylisoborneol from 2MGPP by a mechanism analogous to that employed by (+)-bornyl diphosphate synthase (BPPS) in the cyclization of geranyl diphosphate (GPP) (Figure 1). However, the two cyclization reactions diverge in the final step. While in the BPPS reaction the intermediate secondary bornyl cation is recaptured by the paired pyrophosphate anion (PP_i) on the *endo* face (23-26), in the corresponding MIBS reaction the homologous tertiary 2-methylbornyl cation is quenched by water on the opposite *exo* face (18).

[1]Abbreviations: 2FGPP, 2-fluorogeranyl diphosphate; 2MGPP, 2-methylgeranyl diphosphate; AGPP, 3-aza-2,3-dihydrogeranyl diphosphate; BPPS, (+)-bornyl diphosphate synthase; FPPS, farnesyl diphosphate synthase; GPP, geranyl diphosphate; GSPP, geranyl-*S*-thiolodiphosphate; MIBS, 2-methylisoborneol synthase; PP_i, inorganic pyrophosphate; SAD, single-wavelength anomalous dispersion.

[2]2MGPP is generated by the second enzyme in the operon, the C-methyltransferase 2-methylgeranyl diphosphate synthase (18).

Here, we report the X-ray crystal structures of MIBS from *S. coelicolor* in complex with two different unreactive substrate analogues, geranyl-*S*-thiolodiphosphate (GSPP) and 2-fluorogeranyl diphosphate (2FGPP) (Figure 2).[3] These high resolution structures provide insights regarding the utilization of non-canonical isoprenoid substrates by terpenoid cyclases. Comparisons with BPPS suggest intriguing differences in substrate binding and catalysis, even as these two enzymes generate products that share a core bornyl monoterpene skeleton.

Experimental Procedures

Synthesis of isoprenoid diphosphate ligands

Ligand structures are illustrated in Figure 2. Geranyl-*S*-thiolodiphosphate (GSPP) was purchased from Echelon Biosciences Inc. The synthesis of 2-fluorogeranyl diphosphate (2FGPP) was achieved as previously described (27, 28).

Expression and purification of 2-methylisoborneol synthase (MIBS)

A clone of 2-methylisoborneol synthase from *Streptomyces coelicolor* with a 21-residue hexahistidine tag and linker in pET28a plasmid (Novagen Inc, USA) was described previously (18). This full length MIBS and a truncated variant in which residues M1-P28 were spliced out were expressed using *Escherichia coli* BL21 (DE3) cells (Stratagene Inc.). The truncated variant was initially generated based on the possibility that the actual translational start site for *sco7700* might be at the downstream GTG codon rather than the ATG codon (GTG start codons are relatively common in *Streptomyces*). The truncated variant turned out to be indistinguishable from wild-type MIBS in terms of its kinetics and product distribution. Complete sequences for full length MIBS and the truncated variant used for crystallography are reported in the headers of the corresponding PDB files with accession codes 3V1X and 3V1V, respectively.

Transformed cell cultures were grown in 2 L flasks containing 1 L Lysogeny-Broth medium with 50 mg kanamycin at 37° C. At OD_{600} = 0.6 - 0.7, cultures were equilibrated at 18° C and expression was induced by 0.25 mM isopropyl-1-thio-β-D-galactopyranoside for 16 h. Cells were harvested by centrifugation at 6000*g* for 10 min, producing ~10 g pellet per liter of culture. The pellet was suspended in 20 mL of buffer E (50 mM K_2HPO_4 (pH 7.5), 300 mM NaCl, 10% (v/v) glycerol, 3 mM β-mercaptoethanol) containing 1 mg/mL lysozyme and 1 mM phenylmethylsulfonyl fluoride, then incubated at 4°C for 2 h with shaking. Cells were disrupted by sonication on ice with a large probe at medium power, 10 × (1 min on + 1 min off). Cell debris was cleared by centrifugation twice at 25,000*g* for 45 min. The clear supernatant was applied to a pre-equilibrated Talon column (Clontech Laboratories, CA) at a flow rate of 1 mL/min using an ÄKTAprime plus FPLC system (GE Healthcare Bio-Sciences AB, Sweden). The loaded column was washed with 10 column volumes of buffer E and then with 6 column volumes of buffer E plus 10 mM imidazole. The MIBS protein was eluted with a 100 mL gradient of 10-250 mM imidazole in buffer E at a flow rate of 2.5 mL/min. Selected fractions were combined, concentrated to 10 mL volume, and applied to a Superdex 200 preparative grade 26/60 size exclusion column (GE Healthcare Bio-Sciences AB, Sweden) with buffer M (50 mM piperazine-*N*,*N*′-bis(2-ethanesulfonic acid) (PIPES) (pH 7.0), 10% (v/v) glycerol, 2 mM dithiothreitol, 10 mM $MgCl_2$, and 10 mM NaCl) containing 300 mM NaCl. Fractions from this run were combined, concentrated to a 3 mL volume, and applied to the same column a second time with buffer M. Fractions from the

[3]The atomic coordinates and the crystallographic structure factors of 2-methylisoborneol synthase from *Streptomyces coelicolor* complexed with Mg^{2+}_2-geranyl-*S*-thiolodiphosphate and with Mg^{2+}_2-2-fluorogeranyl diphosphate have been deposited in the Protein Data Bank (www.rcsb.org) with accession codes 3V1V and 3V1X, respectively.

final size exclusion column were combined, concentrated to 5 mg/mL in buffer M, and stored at -80° C.

Crystallization and structure determination of MIBS

Attempts to crystallize MIBS in the absence of ligands were not successful. MIBS was crystallized in the presence of Mg^{2+} and two different isoprenoid ligands by the sitting drop vapor diffusion method. MIBS was incubated at 4° C in the presence of 2.5 mM $MgCl_2$ and 2.5 mM GSPP or 2FGPP overnight before crystallization experiments. Typically, a 1 μL drop of protein solution [10 mg/mL MIBS, 50 mM PIPES (pH 7.0), 10% glycerol, 2 mM dithiothreitol, 12.5 mM $MgCl_2$, 10 mM NaCl, and 2.5 mM isoprenoid ligand] was added to a 1 μL drop of precipitant solution [100 mM Bis-Tris (pH 6.5), 25% polyethylene glycol 3350, 200 mM $(NH_4)_2SO_4$ for the MIBS•GSPP complex; 0.8 M succinic acid (pH 7.0) for the MIBS•2FGPP complex] and equilibrated against a 100 μL reservoir of precipitant solution. Full-length and truncated MIBS were used for the preparation of crystalline MIBS•2FGPP and MIBS•GSPP complexes, respectively. Octahedral crystals appeared within one day and grew to maximal dimensions of 200 μm × 200 μm × 200 μm in 1-2 weeks. Crystals were flash-cooled after transfer to a cryoprotectant solution consisting of the mother liquor augmented with 10% glycerol.

Crystals of the MIBS•GSPP and MIBS•2FGPP complexes diffracted X-rays to 1.80 Å and 1.95 Å resolution at the National Synchrotron Light Source beamline X29A, using incident radiation with λ = 1.008 Å and λ = 1.075 Å, respectively. Crystals of the MIBS•GSPP complex belonged to space group $P4_322$ with unit cell parameters $a = b = 99.39$ Å, $c = 105.74$ Å, α = β = γ = 90°. Crystals of the MIBS•2FGPP complex belonged to space group $P4_322$ with unit cell parameters $a = b = 99.64$ Å, $c = 104.81$ Å, α = β = γ = 90°. Crystals of both complexes contained one monomer in the asymmetric unit with Matthews coefficient $V_M = 2.61 - 2.75$ Å^3/Da (solvent content = 52.8 - 55.2%). For experimental phasing, crystals of the MIBS•GSPP complex were soaked in a cryoprotectant solution [90 mM Bis-Tris (pH 6.5), 22.5% polyethylene glycol 3350, 180 mM $(NH_4)_2SO_4$, 10% glycerol] containing 2 mM methylmercury chloride for 22 h and equilibrated with a 250 μL reservoir of the cryoprotectant solution at 15° C prior to flash-cooling. All necessary safety precautions were taken with regard to the storage, use, and disposal of methylmercury chloride. Single wavelength anomalous dispersion (SAD) data were collected from these crystals at the National Synchrotron Light Source beamline X25, using incident radiation with λ = 1.000 Å. These crystals were isomorphous with those of the MIBS•GSPP complex and diffracted X-rays to 2.1 Å resolution. Diffraction data were processed with HKL2000 (29). Data collection and reduction statistics are recorded in Table 1.

The initial electron density map of the MIBS•GSPP complex was phased by the SAD method. Initially, 5 mercury atoms were located using the program HKL2MAP (30). SAD phasing, search and refinement of 13 additional mercury sites, density modification, initial electron density map calculation, and automatic model building were performed using the AUTOSOL routine implemented in PHENIX (31). This procedure built 62% of the protein residues into the initial electron density map, most of which were contained in α-helices. Manual model building subsequently generated an initial model with 69% of the residues registered in the sequence. This model was used for molecular replacement calculations using the AUTOMR routine implemented in PHENIX with the 1.80 Å resolution data collected from the MIBS•GSPP complex and the 1.95 Å resolution data collected from the MIBS•2FGPP complex. Initial rigid body refinement, iterative cycles of positional refinement, and refinement of the grouped and individual atomic *B*-factors were performed using PHENIX; manual model rebuilding was performed using COOT (32). Water molecules, Mg^{2+} ions, and GSPP or 2FGPP were included in later cycles of refinement. A total of 317 and 311 of 433 and 461 residues are present in the final models of the

MIBS•GSPP and MIBS•2FGPP complexes, respectively. The N-terminal hexahistidine tag, the linker segment, and the proline-rich N-terminal domain (residues M1-A115) were disordered and are absent in the final model. Additional disordered segments include surface loops E155-Q160 and C199-G206. Data reduction and refinement statistics are recorded in Table 1; Ramachandran plot statistics were calculated with PROCHECK (33). Simulated annealing ligand-omit maps were calculated with CNS (34). Protein structure figures were prepared with the graphics program PyMol (http://www.pymol.org) and labeled for publication using PhotoshopCS.

Mutagenesis and Activity Assays

Site-directed mutagenesis studies were performed according to the QuickChange protocol (Qiagen Inc., USA) using the full-length MIBS gene carrying the N-terminal hexahistidine tag and the following mutagenic primers: E193A, CTGATGGTCGCGGCGAACGCGGTGGAC (sense), GTCCACCGCGTTCGCCGCGACCATCAG (antisense); E193D, CTGATGGTCGCGGAC AACGCGGTGGAC (sense), GTCCACCGCGTTGTCCGCGACCATCAG (antisense); E193L, CTGATGGTCGCGCTGAACGCGGTGGAC (sense), GTCCACCGCGTTCAGCGCGACCATCAG (antisense); Y169F, CGGTGGGCCGCTTCATGGTCGGCTG (sense), CAGCCGACCATGAAGCGGCCCACCG (antisense). Mutant genes were verified by DNA sequencing, and mutant proteins were expressed and purified as described above for wild-type MIBS.

For enzyme assays, 5 μM of each MIBS protein (wild-type, E193A, E193D, E193L and Y169F) was incubated separately in 4 mL of assay buffer [50 mM PIPES (pH 7.0), 10 mM $MgCl_2$, 100 mM NaCl, 5 mM β-mercaptoethanol, 20% glycerol] with 60 μM of *E*-2-methylgeranyl pyrophosphate and a 4 mL overlay of pentane for 12 h at 30 °C. The enzymatic products were then extracted with 3 × 4 mL of pentane. The pentane extracts were collected, dried over Na_2SO_4, filtered, concentrated to 100 mL at 0 °C, and analyzed by GC-MS.

The GC-MS analyses were performed using a Hewlett-Packard Series 2 GC-MSD instrument (70 eV, Electron Impact, positive ion mode) and a 30 m × 0.25 mm HP5MS capillary column. The instrument method used was an injection volume of 1 μL, a solvent delay of 3 min and temperature program of 60 °C for 2 min, followed by a temperature gradient of 60-280 °C for 11 min (20 °C min^{-1}) and ending with a 2 min hold at 280 °C. Comparisons of GC-MS detected compounds to their standards were made using the Mass Finder 4.1.40 program (http://www.massfinder.com).

Results and Discussion

Structure of MIBS

The amino acid sequence of MIBS suggests a novel two-domain architecture (18). However, although SDS-PAGE analysis of redissolved crystals confirms that the 13-kDa proline-rich N-terminal domain is retained in the recombinant protein (data not shown), this domain is completely disordered in the crystal based on the absence of well-defined electron density. Molecular disorder for this domain is in fact predicted from the amino acid sequence using the program DISOPRED (35). The function of this unusual domain (>25% proline content), which is present in most MIBS orthologues but is not found in any other terpene synthase, is unknown. The 35-kDa C-terminal domain of MIBS exhibits only 15-23% amino acid sequence identity with the single-domain bacterial and fungal class I sesquiterpene synthases, and the C-terminal domains of plant class I monoterpene and sesquiterpene

synthases, that have yielded crystal structures to date (Table 2). Despite the lack of significant sequence identity to other terpene cyclases, the C-terminal domain of MIBS clearly adopts the class I terpenoid synthase fold (Figure 3).

In the crystal lattice, two molecules of MIBS related by a crystallographic 2-fold axis interact through their C-terminal domains to bury 2565 $Å^2$ surface area, consistent with the formation of a biologically relevant dimer (36). Although dimeric quaternary structure has not previously been reported for MIBS in solution (18-22), the 47 kDa MIBS protein elutes from a gel filtration column as an apparent 80-90 kDa homodimer, while it runs as a ~150 kDa protein in native polyacrylamide gel electrophoresis experiments, indicative of the possibility of even higher order quaternary structure (data not shown).

The active sites in the MIBS dimer are oriented in parallel fashion, and this quaternary structure contrasts with that of all other dimeric terpenoid cyclases that have yielded crystal structures to date (Figure 4). The MIBS dimer assembly is similar, however, to that of farnesyl diphosphate synthase (FPPS) (37), which also has parallel oriented active sites (Figure 4). Even so, the dimer interface in MIBS is formed by helices D1, D2 (including the D1-D2 loop), F, G1, H, and I, whereas in FPPS, helices B, D, E, F, and G1 form the dimer interface. While there are secondary structural elements in common to the dimerization surface of each enzyme, the subunits of the FPPS dimer are rotated ~45° with respect to those of MIBS. In the MIBS dimer, the D1-D2 loop and the D2 helix form a protrusion that prevents dimerization through the same interface as FPPS (Figure 5a). In FPPS, a similar protrusion is formed by helices A and B (Figure 5b).

It is interesting to compare the dimerization interfaces of various terpene synthases that adopt the class I terpenoid synthase fold (Figure 5c). Although dimer interfaces vary from one enzyme to another, dimerization always occurs at the same face of the protein; the opposite face of the protein is reserved for interactions with other domains, such as the disordered proline-rich N-terminal domain of MIBS or the α-helical N-terminal domain of a plant class I cyclase.

The active site of MIBS resides in a deep cavity surrounded by six α helices (C, D, F, G, H, and J). In each enzyme-substrate analogue complex, GSPP and 2FGPP adopt extended conformations in which their diphosphate groups are coordinated to two Mg^{2+} ions, and the distal 6,7-double bond is twisted away from the parallel relationship to the 2,3-allylic double bond that would be required for cyclization of the natural substrate 2MGPP. One metal ion corresponds to the Mg^{2+}_B ion observed in other crystal structures (7) and is coordinated by a water molecule and N345, S349, and E353 in the NSE/DTE motif. The second metal ion is coordinated by five water molecules but no protein residues in the MIBS•2FGPP complex (Figure 6a), or four water molecules and the first residue in the “aspartate-rich” metal-binding motif, D197, in the MIBS•GSPP complex (Figure 6b). This second metal ion corresponds most closely to Mg^{2+}_C in crystal structures of terpenoid cyclases containing a complete trinuclear metal cluster (Figures 6c and 6d) (7). Surprisingly, the “aspartate-rich” motif D^{197}DCYCED at the end of helix D of MIBS is partially disordered and not fully engaged in metal coordination; in other terpene synthase structures, the first aspartate in this motif typically coordinates Mg^{2+}_A and Mg^{2+}_C with syn, synbidentate coordination geometry (7). It is also interesting that the Mg^{2+}_C ion in the MIBS•2FGPP complex appears to be bound with low occupancy. Given the absence of Mg^{2+}_A and the incomplete coordination of Mg^{2+}_C in these complexes, it appears that the active site is incompletely closed. Consistent with an incompletely closed active site, the A-C loop adjacent to the mouth of the active site is disordered, while the C-terminus (i.e., the polypeptide segment following helix J) is ordered but extends away from the mouth of the active site. Helix K, present in other terpenoid cyclases, is absent from MIBS.

Conformational disorder is occasionally but not always observed for short loop segments flanking the mouth of the active site in open or partially-closed conformations of terpenoid cyclases, and such disordered segments usually become ordered upon the binding of 3 metal ions and the substrate/product diphosphate, as recently reviewed (3, 4, 7). We suggest that a fully closed active site would result from the sequential binding of Mg^{2+}_B, Mg^{2+}_C, and Mg^{2+}_A (38), along with the ordering of polypeptide segments flanking the mouth of the active site, as we have previously observed with other terpenoid cyclases (3, 4, 7). Even so, the active site contour of a terpenoid cyclase in an incompletely closed conformation is very similar to that of the cyclase in a fully closed conformation, as we have previously demonstrated for aristolochene synthase from *Aspergillus terreus* (39). Accordingly, mechanistic inferences drawn from the structures of MIBS reported herein are valid.

Mechanistic Implications

MIBS and BPPS generate products with similar bornyl monoterpene skeletons. Numerous biochemical studies of the BPPS mechanism have been reported previously (23-26). Based on the structural similarities between 2-methylisoborneol and (+)-bornyl diphosphate, it follows that MIBS and BPPS share some mechanistic similarities as well. For example, formation of the (4*R*)-α-terpinyl cation leading to bornyl diphosphate and other bicyclic monoterpenes has been shown to require the cisoid-*anti*,*endo*-boat conformation of (3*R*)-linalyl diphosphate, and the stereochemical and regiochemical details of this reaction have been demonstrated using isotopically labeled substrates (25, 26). Accordingly, the organic reaction mechanism outlined for MIBS in Figure 1, involving the corresponding cisoid-*anti*,*endo*-boat conformation of (3*R*)-2-methyllinalyl diphosphate as presented by Wang and Cane (18), builds on the strong mechanistic and stereochemical foundation established for BPPS.

The differences between the respective 2-methylisoborneol and borneol diphosphate products of the reactions catalyzed by MIBS and BPPS arise from the identity and stereochemistry of functional groups attached to the bornyl monoterpene skeleton. Comparisons of the MIBS•GSPP complex and the BPPS•3-aza-2,3-dihydrogeranyl diphosphate (AGPP) complex (40) are useful in understanding the structural basis for these differences. Such comparisons additionally provide useful clues regarding the cyclization reaction catalyzed by *endo*-fenchol synthase, which generates a product with a related norbornyl monoterpene skeleton and shares significant mechanistic features with MIBS and BPPS (Figure 1).

Comparisons of substrate analogue binding modes reveal opposite orientations of the respective diphosphate groups: in the active site of BPPS, the diphosphate group of substrate analogue AGPP coordinates to Mg^{2+}_C through its α-phosphate, whereas in the active site of MIBS, the diphosphate group of the analogue GSPP coordinates to Mg^{2+}_C through its β-phosphate (Figure 7). The inverted orientation of GSPP in the MIBS active site appears to be enabled by structural differences around the G1-G loop that enlarge this side of the active site. In contrast, the opposite side of the active site is more constricted due to the protruding surface of F305, which hinders GSPP from binding with an orientation comparable to that of AGPP in the BPPS•AGPP complex (Figure 7). The isoprenoid conformations in the MIBS•GSPP and BPPS•AGPP complexes are roughly similar, except that the terminal isoprenoid moiety of GSPP is even more extended in its complex with MIBS.

Intriguingly, the extended isoprenoid conformations observed in the MIBS•GSPP and BPPS•AGPP complexes do not correspond to the cisoid-*anti*,*endo*-boat conformation required for cyclization of the (3*R*)-methyllinalyl diphosphate intermediate by BPPS or the (3*R*)-2-methyl-linalyl diphosphate intermediate by MIBS. It should be noted, however, that neither GPP nor 2MGPP are the actual substrates for cyclization – each must first undergo

an enzyme-catalyzed allylic isomerization reaction to form the respective linalyl or 2-methyllinalyl diphosphate intermediate that, after adopting the cisoid-*anti,endo*-boat conformation, undergoes reionization and cyclization. We therefore suggest that the extended isoprenoid conformations of the bound analogues AGPP and GSPP correspond to the productive conformations of GPP and 2MGPP that are required for the initial isomerization reactions catalyzed by BPPS and MIBS, respectively.

It might be considered that incomplete metal binding and active site closure in MIBS is somehow responsible for the extended conformation of GSPP in the MIBS•GSPP complex. However, the extended conformation of AGPP in the BPPS•AGPP complex is observed in the presence of a full complement of 3 Mg^{2+} ions in a fully closed enzyme active site (40). Similarly, an extended substrate analogue conformation is observed in the structure of limonene synthase complexed with 3 Mn^{2+} ions and (3*S*)-2-fluorolinalyl diphosphate enzymatically generated *in situ* by cocrystallizing the enzyme with 2FGPP (27). Thus, the extended conformation of GSPP in its complex with MIBS is not likely to be an artefact of incomplete metal binding. Taken together, the binding conformations of substrate analogues complexed with MIBS, BPPS, and limonene synthase suggest that the extended substrate conformation can be productive for the initial GPP-linalyl diphosphate isomerization reaction catalyzed by these cyclases.

Conformational analysis, including consideration of intramolecular steric interactions, suggests that the conformational change of (3*R*)-linalyl diphosphate or its 2-methyl derivative from the transoid to cisoid conformation must precede the compression of the molecule to the cisoid-*anti,endo*-boat conformation required for cyclization. Otherwise, a steric clash of the H-2 vinylic proton with the 6,7-isoprenoid tail would hinder the requisite 180° rotation about the C-2,3 bond that must occur after initial formation of the *transoid* conformer of (3*R*)-linalyl diphosphate. This intramolecular impediment to rotation would be even more severe for (3*R*)-2-methyl-linalyl diphosphate, since it would involve a steric clash between the C2-methyl group and the 6,7-isoprenoid tail. Thus, the productive conformation for cyclization can differ from that for the initial allylic diphosphate isomerization and *must* be distinct from that for interconversion of the transoid and cisoid conformers of (3*R*)-linalyl diphosphate or (3*R*)-2-methyl-linalyl diphosphate. Even so, the cyclase must exercise sufficient control over productive conformations for isomerization and cyclization so as to prevent alternative conformations that could lead to aberrant cyclization products.

A major chemical difference between the proposed catalytic mechanisms for MIBS and BPPS is found in the final step, in which the 2-methylbornyl or bornyl carbocation intermediate is quenched by the addition of an oxygen nucleophile. In BPPS, the PP_i counterion that is initially released from the GPP substrate and the (3*R*)-linalyl diphosphate intermediate re-adds to the secondary bornyl cation on the *endo* face (Figure 1). By contrast, in MIBS a water molecule attacks the tertiary 2-methylbornyl cation on the *exo* face (Figure 1) (18). The latter reaction is comparable to that catalyzed by (–)-*endo*-fenchol synthase, in which the secondary alcohol has been shown to be derived exclusively by *endo* attack of a water molecule on the fenchyl cation on the face opposite to the PP_i counterion (Figure 1) (41).

If the orientation of the 2-methylbornyl cation bound in the MIBS active site were to be similar to that of 2-azabornane as observed in its complex with BPPS (40), we considered that a residue at the bottom of the active site cleft might serve as a general base to orient a water molecule for nucleophilic addition to the *exo* face of the 2-methylbornyl cation. Indeed, E193 is located at the base of the active site cleft of MIBS, and the presence of a carboxylate side chain is unusual in hydrophobic terpenoid cyclase active sites. Nonetheless, overnight incubation of the E193A, E193L, and E193D mutants with 2MGPP resulted in no

discernible change in either the absolute or relative yields of 2-methylisoborneol and the minor co-product 2-methylenebornane in comparison with the wild-type enzyme (Figures S1, S2). We also tested the role of the nearby residue Y169, but the Y169F mutant similarly exhibited no change in the absolute or relative product yield in an overnight incubation compared with the wild-type enzyme (Figure S3). Thus, neither E193 nor Y169 function as an obligatory general base in catalysis by MIBS. Analysis of the active site cleft does not reveal any alternative amino acid side chains that could serve in this function.

The crystal structure of BPPS complexed with 2-azabornane (a mimic of the 2-bornyl cation), 3 Mg^{2+} ions, and PP_i reveals a trapped water molecule (#110) that makes an exo-oriented hydrogen bond with the amino group of 2-azabornane; this water molecule also hydrogen bonds with Y426 and the PP_i ion (40). The reactivity of this water molecule is hypothesized to account for the formation of olefinic co-products derived from direct deprotonation of carbocation intermediates, as well as hydroxylated products obtained in experiments with GPP analogues (40). If a water molecule were similarly trapped in the active site of MIBS, hydrogen bonded to the PP_i ion and oriented toward the exo face of the 2-methyl-2-bornyl cation, it is possible that the PP_i ion could serve as a general base in activating or orienting the trapped water molecule for nucleophilic addition, or accepting the acidic proton of the resulting hydrated cation. Future structural studies of complexes with analogues of carbocation intermediates may shed additional light on the structural basis for product and stereochemical control in termination of the cyclization cascade catalyzed by MIBS.

Supplementary Material

Refer to Web version on PubMed Central for supplementary material.

Acknowledgments

We thank the National Synchrotron Light Source at Brookhaven National Laboratory for beamline access. We also thank Dr. Chieh-Mei Wang for helpful scientific discussions.

References

1. Davis EM, Croteau R. Cyclization enzymes in the biosynthesis of monoterpenes, sesquiterpenes, and diterpenes. Top in Curr Chem. 2000; 209:53–95.
2. Wendt KU, Schulz GE, Corey EJ, Liu DR. Enzyme mechanisms for polycyclic triterpene formation. Angew Chem Int Ed. 2000; 39:2812–2833.
3. Christianson DW. Structural biology and chemistry of the terpenoid cyclases. Chem Rev. 2006; 106:3412–3442. [PubMed: 16895335]
4. Christianson DW. Unearthing the roots of the terpenome. Curr Op Chem Biol. 2008; 12:141–150.
5. Allemann RK. Chemical wizardry? The generation of chemical diversity in terpenoid biosynthesis. Pure Appl Chem. 2008; 80:1791–1798.
6. Tantillo DJ. The carbocation continuum in terpene biosynthesis – where are the secondary cations? Chem Soc Rev. 2010; 39:2847–2854. [PubMed: 20442917]
7. Aaron JA, Christianson DW. Trinuclear metal clusters in catalysis by terpenoid synthases. Pure Appl Chem. 2010; 82:1585–1597. [PubMed: 21562622]
8. Cane DE, Ikeda H. Exploration and mining of the bacterial terpenome. Acc Chem Res. 2011 in press. 10.1021/ar200198d
9. Cane DE, Tsantrizos YS. Aristolochene synthase. Elucidation of the cryptic germacrene A synthase activity using the anomalous substrate dihydrofarnesyl diphosphate. J Am Chem Soc. 1996; 118:10037–10040.
10. Miller DJ, Yu F, Allemann RK. Aristolochene synthase-catalyzed cyclization of 2-fluorofarnesyl-diphosphate to 2-fluorogermacrene A. Chem Bio Chem. 2007; 8:1819–1825.

11. Miller DJ, Yu F, Knight DW, Allemann RK. 6- and 14-Fluoro farnesyl diphosphate: mechanistic probes for the reaction catalysed by aristolochene synthase. Org Biomol Chem. 2009; 7:962–975. [PubMed: 19225680]
12. Vedula LS, Zhao Y, Coates RM, Koyama T, Cane DE, Christianson DW. Exploring biosynthetic diversity with trichodiene synthase. Arch Biochem Biophys. 2007; 466:260–266. [PubMed: 17678871]
13. Buttery RG, Garibaldi JA. Geosmin and methylisoborneol in garden soil. J Agric Food Chem. 1976; 24:1246–1247.
14. Martin JF, Bennett LW, Graham WH. Off-flavor in the channel catfish (*Ictalurus punctatus*) due to 2-methylisoborneol and its dehydration products. Water Sci Technol. 1988; 20:99–105.
15. McCallum R, Pendleton P, Schumann R, Trinh MU. Determination of geosmin and 2-methylisoborneol in water using solid-phase microextraction and gas chromatography-chemical ionisation/electron impact ionisation-ion-trap mass spectrometry. Analyst. 1998; 123:2155–2160. [PubMed: 10209901]
16. Jüttner F, Watson SB. Biochemical and ecological control of geosmin and 2-methylisoborneol in source waters. Appl Environ Microbiol. 2007; 73:4395–4406. [PubMed: 17400777]
17. Karahadian C, Josephson DB, Lindsay RC. Volatile compounds from *Penicillium* sp. contributing musty-earthy notes to Brie and Camembert cheese flavors. J Agric Food Chem. 1985; 33:339–343.
18. Wang CM, Cane DE. Biochemistry and molecular genetics of the biosynthesis of the earthy odorant methylisoborneol in *Streptomyces coelicolor*. J Am Chem Soc. 2008; 130:8908–8909. [PubMed: 18563898]
19. Komatsu M, Tsuda M, Omura S, Oikawa H, Ikeda H. Identification and functional analysis of genes controlling biosynthesis of 2-methylisoborneol. Proc Natl Acad Sci USA. 2008; 105:7422–7427. [PubMed: 18492804]
20. Chou WK, Ikeda H, Cane DE. Cloning and characterization of Pfl_1841, a 2-methylenebornane synthase in *Pseudomonas fluorescens* PfO-1. Tetrahedron. 2011; 67:6627–6632. [PubMed: 21804650]
21. Giglio S, Chou WK, Ikeda H, Cane DE, Monis PT. Biosynthesis of 2-methylisoborneol in cyanobacteria. Environ Sci Technol. 2011; 45:992–998. [PubMed: 21174459]
22. Wang Z, Xu Y, Shao J, Wang J, Li R. Genes associated with 2-methylisoborneol biosynthesis in cyanobacteria: isolation, characterization, and expression in response to light. PLoS ONE. 2011; 6:e18665.10.1371/journal.pone.0018665 [PubMed: 21490938]
23. Cane DE, Saito A, Croteau R, Shaskus J, Felton M. Enzymic cyclization of geranyl pyrophosphate to bornyl pyrophosphate. Role of the pyrophosphate moiety. J Am Chem Soc. 1982; 104:5831–5833.
24. Croteau RB, Shaskus JJ, Renstrøm B, Felton NM, Cane DE, Saito A, Chang C. Mechanism of the pyrophosphate migration in the enzymic cyclization of geranyl and linalyl pyrophosphates to (+)- and (-)-bornyl pyrophosphates. Biochemistry. 1985; 24:7077–7085. [PubMed: 4084562]
25. Croteau R, Felton NM, Wheeler CJ. Stereochemistry at C-1 of geranyl pyrophosphate and neryl pyrophosphate in the cyclization to (+)- and (-)-bornyl pyrophosphate. J Biol Chem. 1985; 260:5956–5962. [PubMed: 3997807]
26. Wise ML, Pyun HJ, Helms G, Assink B, Coates RM, Croteau RB. Stereochemical disposition of the geminal dimethyl groups in the enzymatic cyclization of geranyl diphosphate to (+)-bornyl diphosphate by recombinant (+)-bornyl diphosphate synthase from *Salvia officinalis*. Tetrahedron. 2001; 57:5327–5334.
27. Hyatt DC, Youn B, Zhao Y, Santhamma B, Coates RM, Croteau RB, Kang CH. Structure of limonene synthase, a simple model for terpenoid cyclase catalysis. Proc Natl Acad Sci USA. 2007; 104:5360–5365. [PubMed: 17372193]
28. Karp F, Zhao Y, Santhamma B, Assink BK, Coates RM, Croteau RB. Inhibition of monoterpene cyclases by inert analogues of geranyl diphosphate and linalyl diphosphate. Arch Biochem Biophys. 2007; 468:140–146. [PubMed: 17949678]
29. Otwinowski Z, Minor W. Processing of X-ray diffraction data collected in oscillation mode. Methods Enzymol. 1997; 276:307–326.

30. Pape T, Schneider TR. HKL2MAP: a graphical user interface for phasing with SHELX programs. J Appl Cryst. 2004; 37:843–844.

31. Adams PD, Afonine PV, Bunkóczi G, Chen VB, Davis IW, Echols N, Headd JJ, Hung LW, Kapral GJ, Grosse-Kunstleve RW, McCoy AJ, Moriarty NW, Oeffner R, Read RJ, Richardson DC, Richardson JS, Terwilliger TC, Zwart PH. PHENIX: a comprehensive Python-based system for macromolecular structure solution. Acta Crystallogr. 2010; D66:213–221.

32. Emsley P, Lohkamp B, Scott WG, Cowtan K. Features and development of Coot. Acta Crystallogr. 2010; D66:486–501.

33. Laskowski RA, MacArthur MW, Moss DS, Thornton JM. PROCHECK: A program to check the stereochemical quality of protein structures. J Appl Cryst. 1993; 26:283–291.

34. Brünger AT, Adams PD, Clore GM, DeLano WL, Gros P, Grosse-Kunstleve RW, Jiang JS, Kuszewski J, Nilges M, Pannu NS, Read RJ, Rice LM, Simonson T, Warren GL. Crystallography & NMR System: A new software suite for macromolecular structure determination. Acta Crystallogr. 1998; D54:905–921.

35. Ward JJ, Sodhi JS, McGuffin LJ, Buxton BF, Jones DT. Prediction and functional analysis of native disorder in proteins from the three kingdoms of life. J Mol Biol. 2004; 337:635–645. [PubMed: 15019783]

36. Krissinel E, Henrick K. Inference of macromolecular assemblies from crystalline state. J Mol Biol. 2007; 372:774–797. [PubMed: 17681537]

37. Tarshis LC, Yan M, Poulter CD, Sacchettini JC. Crystal structure of recombinant farnesyl diphosphate synthase at 2.6-Å resolution. Biochemistry. 1994; 33:10871–10877. [PubMed: 8086404]

38. Shishova EY, Yu F, Miller DJ, Faraldos JA, Zhao Y, Coates RM, Allemann RK, Cane DE, Christianson DW. X-ray crystallographic studies of substrate binding to aristolochene synthase suggest a metal ion binding sequence for catalysis. J Biol Chem. 2008; 283:15431–15439. [PubMed: 18385128]

39. Shishova EY, Di Costanzo L, Cane DE, Christianson DW. X-ray crystal structure of aristolochene synthase from *Aspergillus terreus* and the evolution of templates for the cyclization of farnesyl diphosphate. Biochemistry. 2007; 46:1941–1951. [PubMed: 17261032]

40. Whittington DA, Wise ML, Urbansky M, Coates RM, Croteau RB, Christianson DW. Bornyl diphosphate synthase: structure and strategy for carbocation manipulation by a terpenoid cyclase. Proc Natl Acad Sci USA. 2002; 99:15375–15380. [PubMed: 12432096]

41. Croteau R, Shaskus J, Cane DE, Saito A, Chang C. Enzymic cyclization of [1-^{18}O]geranyl pyrophosphate to *l-endo*-fenchol. J Am Chem Soc. 1984; 106:1142–1143.

42. Hong YJ, Tantillo DJ. Quantum chemical dissection of the classic terpinyl/pinyl/bornyl/camphyl cation conundrum-the role of pyrophosphate in manipulating pathways to monoterpenes. Org Biomol Chem. 2010; 8:4589–4600. [PubMed: 20725661]

43. Weitman M, Major DT. Challenges posed to bornyl diphosphate synthase: diverging reaction mechanisms in monoterpenes. J Am Chem Soc. 2010; 132:6349–6360. [PubMed: 20394387]

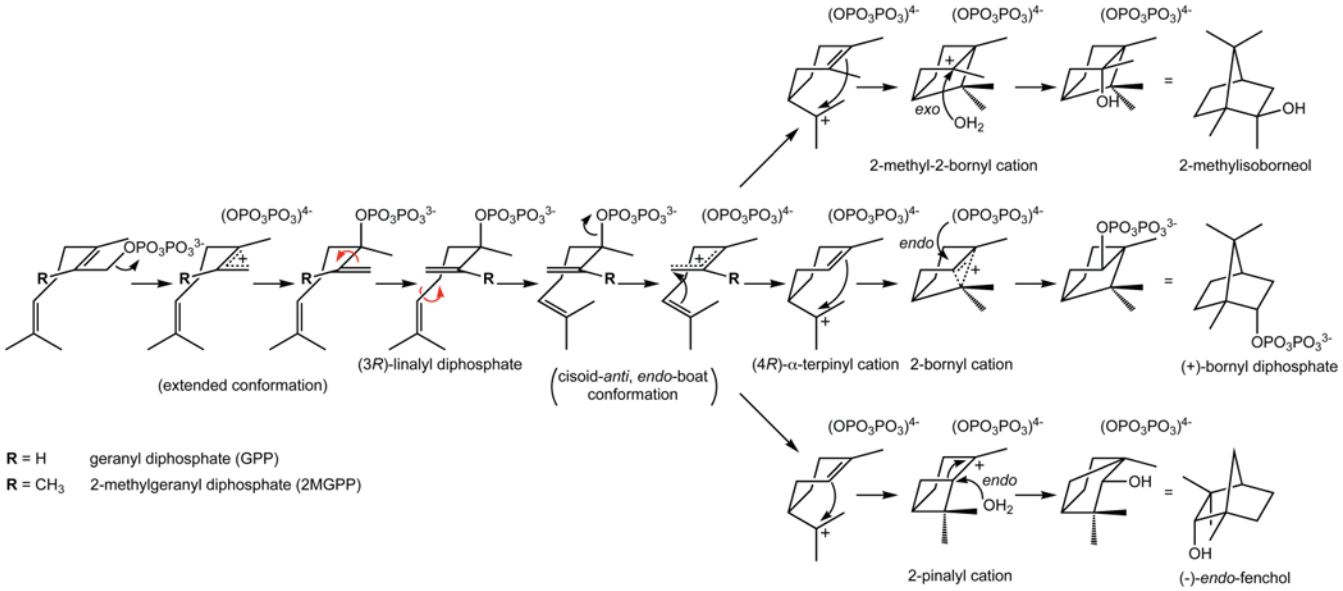

Figure 1.

Proposed cyclization mechanisms of MIBS (18), (+)-bornyl diphosphate synthase (23-26), and *endo*-fenchol synthase (41). Common to each mechanism are conformational changes (red arrows) in the (3*R*)-linalyl diphosphate intermediate (or its 2-methyl derivative) leading to the cisoid-*anti*, *endo*-boat conformation required for cyclization. The conversion of the (4*R*)-α-terpinyl cation to (+)-bornyl diphosphate could occur in a single, concerted step or through a nonclassical carbonium ion to avoid formation of the 2-bornyl cation, a relatively unstable secondary carbocation (23, 42, 43).

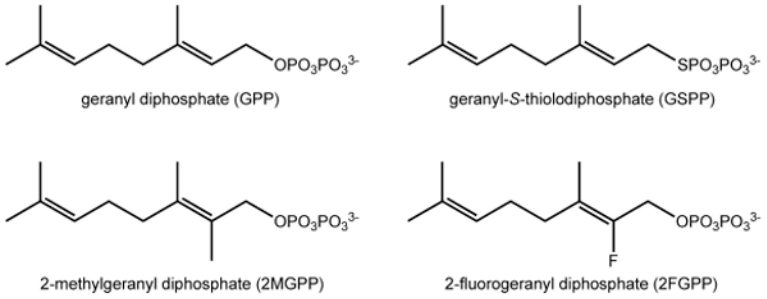

Figure 2.
Substrates utilized by MIBS and their unreactive analogues.

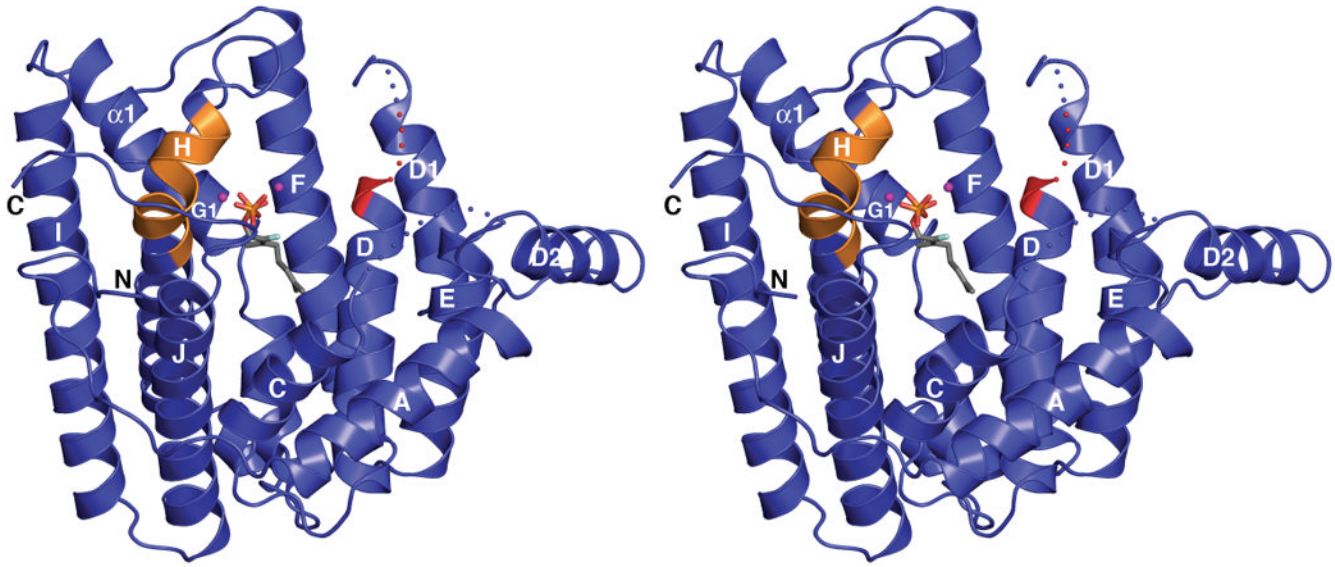

Figure 3.

The 35-kDa C-terminal catalytic domain of MIBS adopts the α-helical class I terpenoid synthase fold as shown, and the 13-kDa proline-rich N-terminal domain is disordered and hence not shown. The N- and C-termini are labeled with black letters, and the D^{197}DCYCED and N^{345}DLYSYTKE metal-binding motifs are red and orange, respectively. Disordered polypeptide segments are indicated by dotted lines. The active site is indicated by the binding of 2FGPP (stick figure) and two Mg^{2+} ions (small magenta spheres).

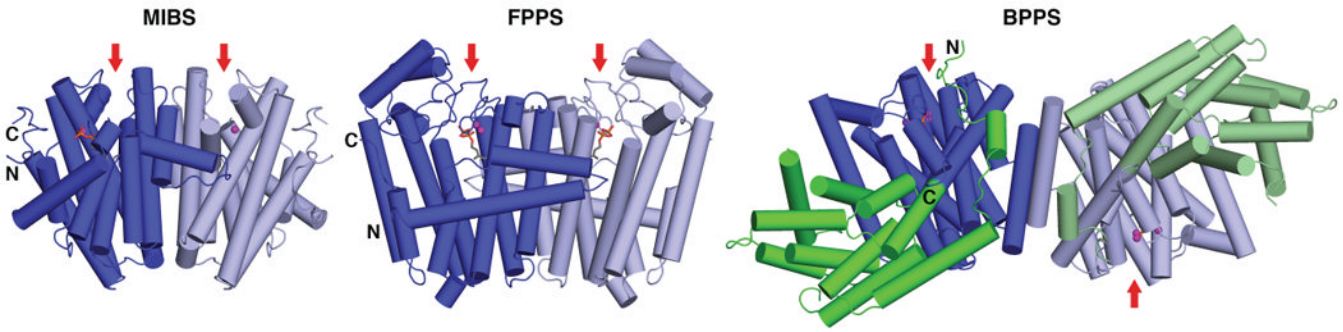

Figure 4.

Dimeric quaternary structures of MIBS, farnesyl diphosphate synthase from *Gallus gallus* (FPPS; PDB ID: 1UBW), and (+)-bornyl diphosphate synthase from *Salvia officinalis* (BPPS; PDB ID: 1N20). The catalytic C-terminal domain, which forms the dimerization interface, is dark/light blue; the N-terminal domain of BPPS is dark/light green. A red arrow indicates the mouth of each active site. The active sites in the MIBS dimer are oriented in parallel fashion, like those in the FPPS dimer. The active sites in the BPPS dimer are oriented in antiparallel fashion, which is the case for all structures of terpenoid cyclase dimers determined to date.

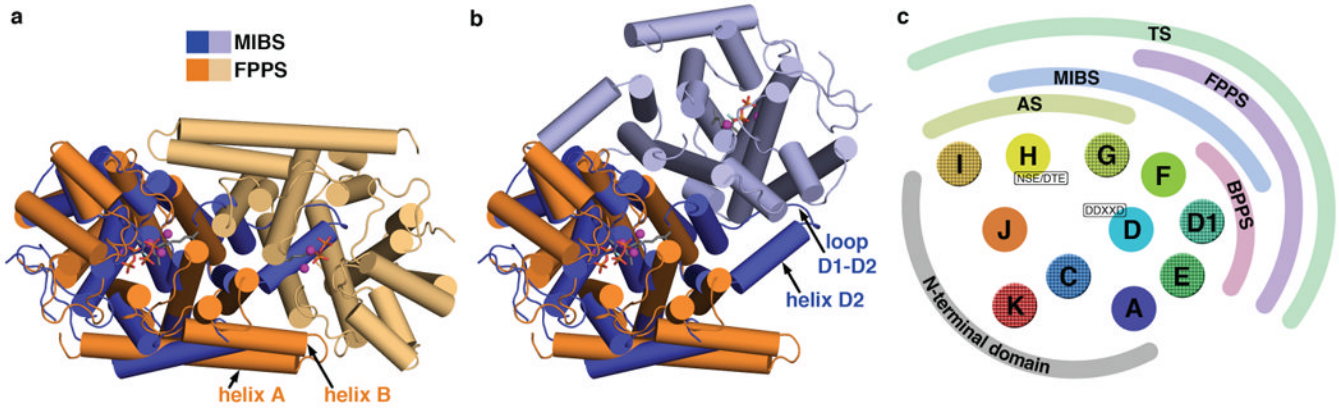

Figure 5.

Comparison of MIBS and FPPS dimer assembly. (a) Superposition of the FPPS dimer (orange/tan) on one monomer of MIBS (blue); for reference, active sites are indicated by bound ligands. Helices A and B are elongated in FPPS and guide dimer assembly. The protrusion of helix D2 and the D1-D2 loop would block the comparable assembly of the MIBS dimer. (b) Superposition of the MIBS dimer (blue/light blue) on one monomer of FPPS (orange); for reference, active sites are indicated by bound ligands. The protruding helix D2 and the D1-D2 loop help define a surface for dimer assembly that is absent in FPPS. (c) Schematic diagram of the class I terpenoid synthase fold showing the general interfaces utilized by various members of the class for dimerization. Major helices are indicated by circles colored in “rainbow” sequence from the N-terminus (blue) to the C-terminus (red). Circles with solid colors represent helices with their C-termini directed toward the viewer; those with cross-hatching represent helices that are directed away from the viewer. Metal-binding motifs on helices D and H are also indicated. If a second domain is present, such as the proline-rich domain of MIBS or the non-functional N-terminal domain of BPPS, it would interact with the side opposite that of the dimerization surface, as indicated.

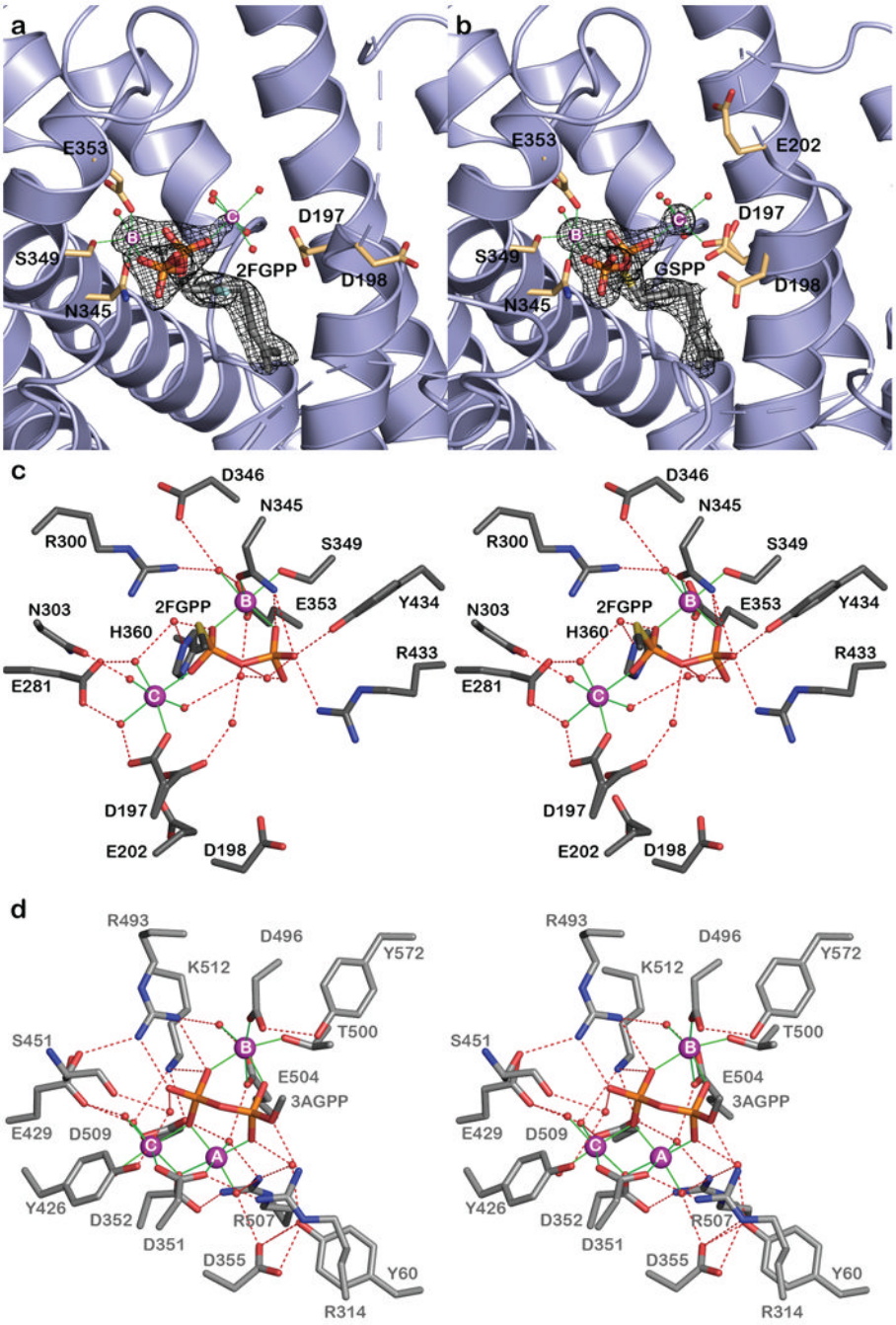

Figure 6.

Substrate analogue binding to MIBS. (a) Simulated annealing omit maps showing the binding of 2FGPP (contoured at 4σ) and two Mg^{2+} ions (contoured at 4σ) in the active site of MIBS. Weak electron density for $Mg^{2+}{}_C$ suggests partial occupancy. Side chains of key residues in the D^{197}DCYCED and N^{345}DLYSYTKE motifs are displayed as stick figures and metal coordination interactions are indicated by green dotted lines. Disordered polypeptide segments appear as broken lines. (b) Simulated annealing omit maps showing the binding of GSPP (contoured at 4σ) and two Mg^{2+} ions (contoured at 4σ) in the active site of MIBS. Side chains of key residues in the D^{197}DCYCED and N^{345}DLYSYTKE motifs are displayed as stick figures and metal coordination interactions are indicated by

green dotted lines. Disordered polypeptide segments appear as broken lines. (c) Stereoview of the MIBS•2FGPP complex; for clarity, only one carbon atom of the isoprenoid group is shown to indicate its connectivity with the diphosphate group. Selected active site residues are indicated; metal coordination and hydrogen bond interactions are indicated by green lines and red dashed lines, respectively. Atoms are color-coded as follows: carbon = dark gray, nitrogen = blue, oxygen = red, sulfur = yellow, phosphorus = orange; Mg^{2+} ions and water molecules appear as magenta spheres and red spheres, respectively. (d) Stereoview of the BPPS•AGPP complex (gray, PDB 1N20); for clarity, only one carbon atom of the isoprenoid group is shown to indicate its connectivity with the diphosphate group. Atomic color coding is the same as in (c) except that carbon = light gray. In contrast with the MIBS•2FGPP complex, the BPPS•AGPP complex contains a complete trinuclear metal cluster.

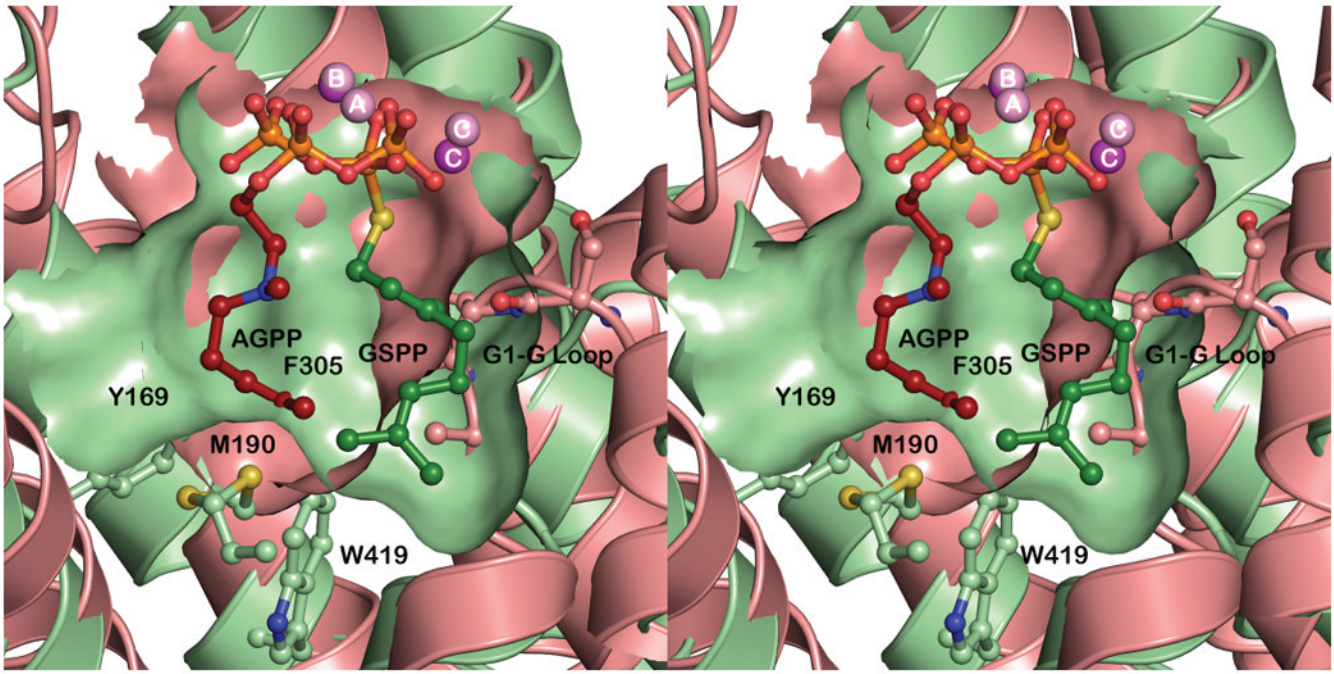

Figure 7.

Stereographic cut-away view of superimposed active site contours of MIBS (green) and BPPS (pink, PDB ID: 1N20). Geranyl diphosphate analogues GSPP and AGPP are shown as ball-and-stick figures in darker shades, and selected amino acid side chains are indicated.

Table 1
Data Collection and Refinement Statistics

	MIBS-Mg^{2+}_2-GSPP complex	MIBS-Mg^{2+}_2-2FGPP complex
A. *Data Collection*		
Incident wavelength (Å)	1.008	1.075
Resolution range (Å)	50.0-1.80	50.0-1.95
No. of reflections (total/unique)	510238/49647	353502/37222
Redundancy[a]	10.3 (9.1)	9.5 (8.6)
Completeness[a] (%)	100 (100)	95.9 (93.6)
I/σ	23.7 (4.5)	14.3 (2.5)
R_{merge}[b]	0.099 (0.495)	0.128 (0.849)
B. *Refinement*		
R_{work}/R_{free}[c]	0.150 / 0.176	0.176 / 0.219
Protein atoms[d]	2573	2490
Solvent atoms[d]	426	250
Ligand atoms[d]	28	22
R.m.s. deviations		
Bonds (Å)	0.029	0.022
Angles (°)	2.2	1.8
Dihedral angles (°)	19.1	17.9
Improper dihedral angles (°)	3.1	1.9
Average B factors (Å^2)		
Main chain	18	29
Side chain	21	32
Ligand	27	34
Solvent	32	35
Ramachandran plot		
Allowed (%)	94.5	95.1
Additionally allowed (%)	5.5	4.5
Generously allowed (%)	0	0.4
Disallowed (%)	0	0

[a] Number in parentheses refer to the outer shell of data.

[b] $R_{merge} = \Sigma|I-\langle I\rangle|/\Sigma I$, where I is the observed intensity and $\langle I\rangle$ is the average intensity calculated from replicate data.

[c] $R_{work} = \Sigma| |F_O| - |F_C| | / \Sigma|F_O|$ for reflections contained in the working set, and $R_{free} = \Sigma| |F_O| - |F_C| | / \Sigma|F_O|$ for reflections contained in the test set held aside during refinement (1% of the total number of reflections). $|F_O|$ and $|F_C|$ are the observed and calculated structure factor amplitudes, respectively.

[d] Per asymmetric unit.

Table 2

Comparison of MIBS with mono- and sesquiterpene cyclases of known structure

	Classification	Sequence identity (%)	C_α r.m.s. deviation (Å)[a]	Aspartate-rich motif[b]	NSE/DTE motif[b]
MIBS	bacterial, C_{11}	-	-	**D**^{197}DCYCED	**N**^{345}DLY**S**YTK**E**
pentalenene synthase	bacterial, C_{15}	20	2.1 (252)	D^{80}DLFD	N^{219}DIASLEKE
epi-isozizaene synthase	bacterial, C_{15}	23	2.2 (260)	**D**^{99}DRH**D**	**N**^{240}DLC**S**LPK**E**
aristolochene synthase	fungal, C_{15}	18	2.8 (223)	D^{115}DVLE	N^{244}DIYSYDKE
aristolochene synthase	fungal, C_{15}	20	3.2 (243)	**D**^{90}DLL**E**	**N**^{219}DIY**S**YEK**E**
trichodiene synthase	fungal, C_{15}	16	3.4 (243)	**D**^{100}DSK**D**	**N**^{225}DLM**S**FYK**E**
(+)-bornyl diphosphate	plant, C_{10}	16	2.5 (245)	**D**^{351}DIY**D**	**D**^{496}DLG**T**SYF**E**
limonene synthase	plant, C_{10}	15	2.4 (240)	**D**^{352}DIY**D**	**D**^{496}DLG**T**SVE**E**
cineole synthase	plant, C_{10}	15	2.4 (233)	**D**^{345}DVF**D**	**D**^{489}DMG**T**SLD**E**
epi-aristolochene	plant, C_{15}	18	2.5 (247)	**D**^{301}DTF**D**	**D**^{444}DTA**T**YEV**E**
δ-cadinene synthase	plant, C_{15}	15	2.5 (240)	**D**^{307}DTY**D**	**D**^{451}DVA**E**HKFK

[a] Number of C_α atoms aligned in the class I terpenoid cyclase domains are shown in parentheses.

[b] Residues that coordinate to metal ions in crystal structures of enzyme-ligand complexes are in boldface. Note that no enzymemetal-ligand complex has been prepared to date with pentalenene synthase and aristolochene synthase from *Penicillium roqueforti*.